


EXPRESS LETTER

Open Access



Electrical resistivity modeling around the Hidaka collision zone, northern Japan: regional structural background of the 2018 Hokkaido Eastern Iburi earthquake (M_w 6.6)

Hiroshi Ichihara^{1*} , Toru Mogi^{1,2,3}, Hideyuki Satoh⁴ and Yusuke Yamaya⁵

Abstract

The Hidaka collision zone, the collision boundary between the NE Japan and Kurile arcs, is known to be an ideal region to study the evolution of island arcs. The hypocenter of the 2018 Hokkaido Eastern Iburi earthquake (M_w 6.6) in the western part of the Hidaka collision zone was unusually deep for an inland earthquake, and the reverse fault that caused the earthquake has an uncharacteristically steep dip. In this study, we used three-dimensional inversion to reanalyze broadband magnetotelluric data acquired in the collision zone. The inverted resistivity model showed a significant area of high resistivity around the center of the collision boundary. We also identified a conductive zone beneath an area of serpentinite mélangé in a zone of high P – T metamorphic rocks west of the high-resistivity zone. The conductive zone possibly reflects areas rich in pore fluids related to the formation and elevation of the serpentinites. Sensitivity tests indicated the need for additional magnetotelluric survey data to delineate the resistivity distribution around the epicentral area of the 2018 earthquake although the resistivity model showed a conductive zone in this area.

Keywords: Hidaka collision zone, Magnetotellurics, Electrical conductivity, Resistivity, Serpentinite, 2018 Hokkaido Eastern Iburi earthquake

Introduction

The Hidaka collision zone (HCZ) is generally recognized as an ideal area for research on crustal evolution in subduction systems. The obliquely subducting Pacific plate drives westward migration of the forearc sliver of the Kurile arc, which results in obduction of the sliver onto the NE Japan arc (e.g., Kimura 1986) (Fig. 1a). The obduction has exposed the low- P – T metamorphic and plutonic rocks of the Hidaka metamorphic belt east of the Hidaka main thrust (HMT) (Fig. 1b). In the NE Japan arc on the

western side of the HMT, metamorphosed accretionary complexes that formed under high P – T conditions (Kamui-kotan belt) are distributed between Cretaceous sedimentary rocks. The Kamui-kotan belt is characterized by ultramafic rock bodies, mainly serpentinite mélangé. However, the mechanism that elevated these rocks is not well understood (e.g., Ueda 2006). West of the Kamui-kotan belt, the collision has resulted in the formation of foreland fold-and-thrust structures in the thick sequence of Cretaceous to Neogene sedimentary rocks, thus providing an ideal area for research on crustal shortening (e.g., Kato et al. 2004). Therefore, further investigation of crustal structures is essential to understand the tectonics around the HCZ.

The 2018 Hokkaido Eastern Iburi earthquake (M_w 6.6) occurred near the western edge of the HCZ and

*Correspondence: h-ichi@seis.nagoya-u.ac.jp

¹ Earthquake and Volcano Research Center, Graduate School of Environmental Studies, Nagoya University, Furo-cho, Chikusa-ku, Nagoya 464-8601, Japan

Full list of author information is available at the end of the article

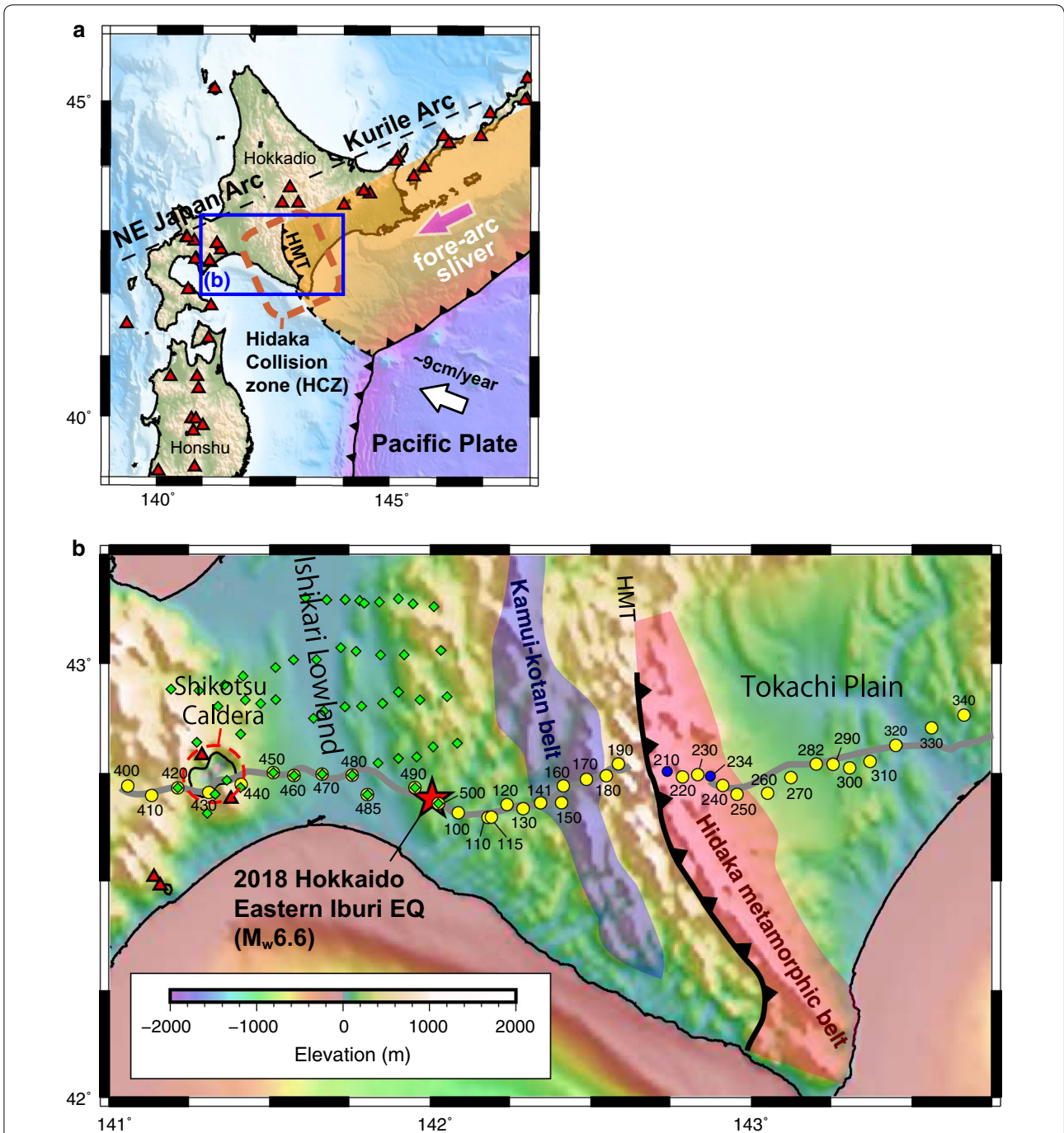


Fig. 1 Maps showing locations of the study area and MT stations. **a** Tectonic setting of the Hokkaido region showing the study area. Red triangles denote active volcanoes. **b** Map of the study area showing simplified local geology and the locations of MT stations. Yellow and blue circles denote MT stations used in 2000–2001 and 2005, respectively. Green diamonds are MT stations used in resistivity modeling by Yamaya et al. (2017). Note that MT data from stations 420 and 450–500 were used in the 3-D inversions of both this study and that of Yamaya et al. (2017). The gray line marks the seismic refraction/wide-angle reflection profile of Iwasaki et al. (2004). The background elevation image was constructed from the ETOPO1 global relief model (Amante and Eakins 2009)

caused devastating damage and 41 fatalities. The estimated hypocentral depth of 37 km is anomalously deep because it significantly exceeds the depth of the brittle–ductile boundary (e.g., Scholz 2002). Although the focal mechanism indicates that the earthquake was caused by reverse faulting, the distribution of after-shock hypocenters indicates that the fault dips about 80°E (Japan Meteorological Agency 2019). This fault orientation is uncharacteristic of reverse faulting but can be explained by high pore fluid pressure in the fault zone (e.g., Sibson 1990). Kita et al. (2012) identified a steep seismic velocity boundary along another anomalously deep earthquake fault in the HCZ (1982 Urakawa-oki earthquake, M_w 6.9), which might be associated with enhancement of the fault rupture. Thus, geophysical imaging is essential to further investigate the deep faulting in the HCZ. Because electrical resistivity data can constrain fluid and temperature distributions that control fault behavior and the depth of the brittle–ductile boundary, examination of these data should contribute to our understanding of these anomalous features of reverse faulting in the HCZ.

Yamaya et al. (2017) proposed a subsurface 3-D resistivity model for the area around the Ishikari Plain based on their MT observations and some of the MT data acquired by Mogi and Hidaka 2000 MT Group (2002) (Fig. 1). Their model showed remarkable conductors beneath the Shikotsu caldera and Ishikari-Teichi-Toen fault, which implied the presence of magmatic fluid under the former and aqueous fluid under the latter. However, structures around the center of the HCZ and the focal area of the 2018 Hokkaido Eastern Iburu Earthquake have not yet been clearly elucidated by 3-D magnetotelluric (MT) resistivity modeling.

In this study, we estimated the resistivity distribution beneath a long MT survey transect through the HCZ between the volcanic front of the NE Japan arc and the Tokachi plain of the Kurile arc (Fig. 1b). Although Mogi and Hidaka 2000 MT Group (2002) used 2-D inversion to construct a preliminary resistivity model along this transect, the MT data indicated strong three-dimensionality (see “[Magnetotelluric data and impedance](#)” and “[Phase tensor and induction vectors](#)” sections), so a robust resistivity model has not yet been estimated. We therefore applied 3-D inversion to the resistivity data acquired by Mogi and Hidaka 2000 MT Group (2002) and interpreted the inversion results to gain an understanding of the 2018 Hokkaido Eastern Iburu earthquake and the tectonics of the HCZ.

Observations and analyses

Magnetotelluric data and impedance

We used broadband MT data acquired at 36 sites by the Mogi and Hidaka 2000 MT Group (2002) in 2000–2001 (Fig. 1b). The MT stations were located at 4–10 km intervals along a survey line previously used to acquire seismic refraction and wide-angle reflection data (Iwasaki et al. 2004). We also acquired broadband MT data in 2005 at two sites in the Hidaka metamorphic belt where coverage of the 2000–2001 survey data was sparse (Fig. 1b). All of the data were recorded using MTU-5 systems manufactured by Phoenix Geophysics Ltd. Three orthogonal components of the magnetic field were acquired using induction coils, and two horizontal components of the electric field were acquired using Pb–PbCl₂ electrodes. The duration of data acquisition at each site was 2–6 days.

Magnetotelluric impedance tensors and geomagnetic transfer functions were estimated using an SSMT-2000 system supplied by Phoenix Geophysics Ltd. To reduce local electromagnetic field noise, we applied the remote reference technique of Gamble et al. (1979) using the horizontal component of magnetic field data. The remote data for the 2000–2001 survey were recorded simultaneously with the main dataset, but at a different MT site on the survey line. For remote reference data for the 2005 MT data, we used horizontal geomagnetic field data acquired by the MTU-5 system at the Esashi geomagnetic observatory, which is operated by the Geospatial Information Authority of Japan.

The calculated MT impedance tensors, which were converted to apparent resistivity and impedance phase (Fig. 2, Additional file 1), showed considerable variation. Apparent resistivities were low ($<10 \Omega\text{m}$) beneath the Ishikari lowland and Tokachi Plain, but were high beneath the Hidaka metamorphic belt. The impedance phases showed out-of-quadrant phases in off-diagonal components at a few sites around the Shikotsu Caldera and Hidaka metamorphic belt (e.g., sites 420 and 230 in Fig. 2). The out-of-quadrant phases possibly represent the combined effect of two anisotropic layers, each with a different anisotropic azimuth (e.g., Pek and Verner 1997; Heise and Pous 2003), or channeling and bending of the telluric current that requires resolution by 3-D resistivity modeling (e.g., Ichihara and Mogi 2009; Ichihara et al. 2013).

Phase tensor and induction vectors

We calculated the phase tensor (Caldwell et al. 2004) and Parkinson's induction vector (Parkinson 1962) to evaluate the dimensionality and trend of the resistivity structure. The phase tensor is a second-rank tensor

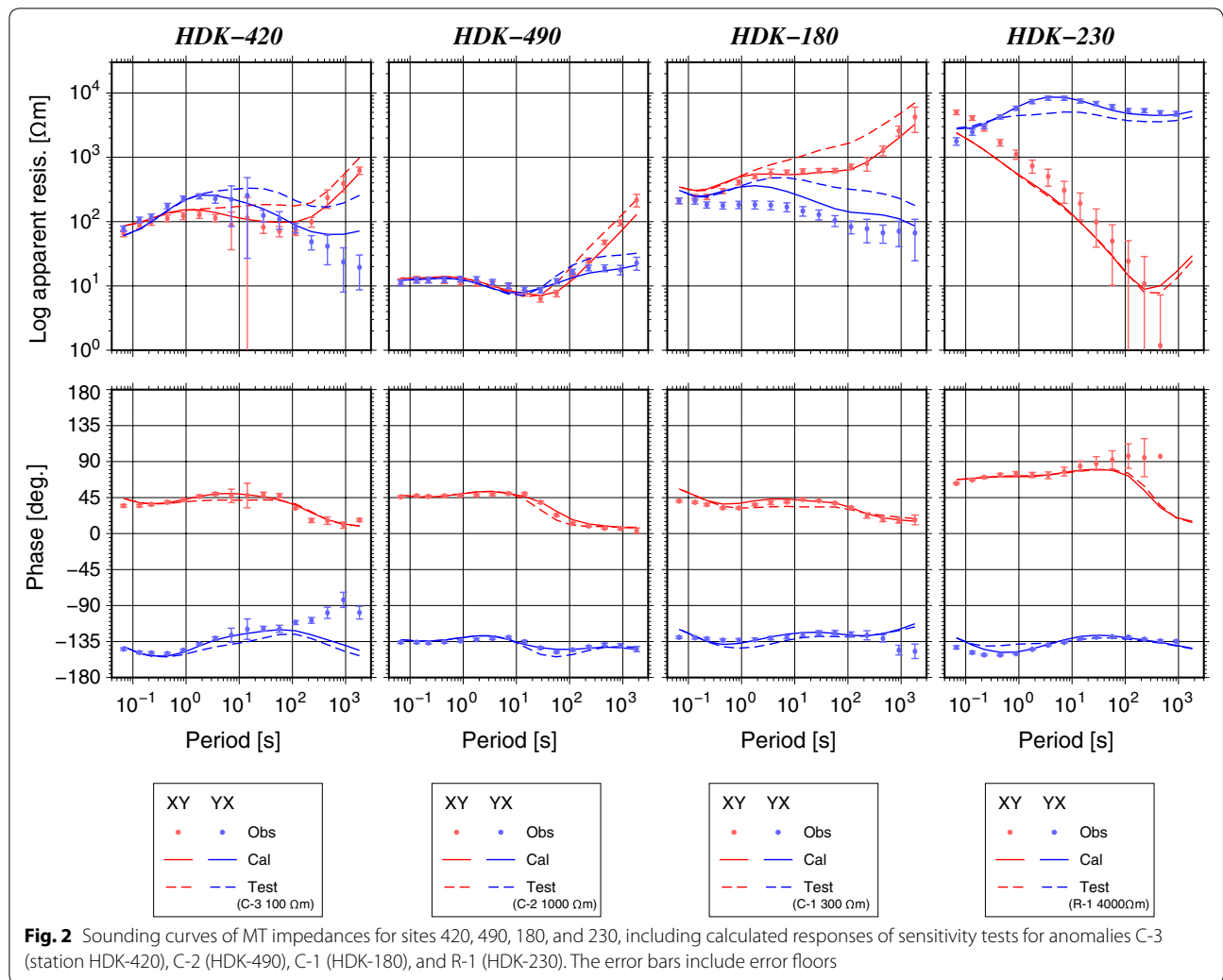


Fig. 2 Sounding curves of MT impedances for sites 420, 490, 180, and 230, including calculated responses of sensitivity tests for anomalies C-3 (station HDK-420), C-2 (HDK-490), C-1 (HDK-180), and R-1 (HDK-230). The error bars include error floors

that describes the phase relationship contained in the MT impedance tensor (Caldwell et al. 2004). It preserves the effect of regionally heterogeneous resistivity, whereas the MT impedance tensor is distorted by the galvanic effects produced by heterogeneity of near surface resistivity. The root of the determinant of the phase tensor is called Φ_2 . In the simple 1-D case, $\Phi_2 > 45^\circ$ and $\Phi_2 < 45^\circ$ indicate decreasing and increasing resistivity, respectively, with increasing depth.

The phase tensor ellipses showed high Φ_2 values ($> 60^\circ$) at 0.222 s under the Ishikari lowland and Tokachi Plain, but low values ($< 30^\circ$) in these areas at 56.8 s (Fig. 3, Additional file 2). These observations indicate that the shallow resistivity decreased with depth, whereas the deep resistivity increased with depth. In the area of the Hidaka metamorphic belt, high Φ_2 ($> 50^\circ$) was estimated between 3.56 and 56.8 s, implying decreasing resistivity with depth.

The azimuths of the principal axes of phase tensor ellipses, which indicate the azimuth of strike (or azimuth perpendicular to strike) of a resistivity structure in a 2-D model, were mostly aligned at 330° at 909 s. However, the azimuths of the principal axes varied considerably at shorter periods, indicating that the shallow electrical resistivity structure has strong three-dimensionality. Absolute values of skew angle (β) were large ($> 5^\circ$) at periods longer than 56.8 s at more than half of the MT sites, which is also an indicative of strong three-dimensionality. Negative values of β at 56.8 s near the HCZ had become positive at 909 s, which implies an asymmetric resistivity distribution.

The Parkinson's induction vector is defined as the reverse vector of the real part of the geomagnetic transfer function, and it commonly points to a conductive anomaly (Parkinson 1962). Parkinson's induction vectors between 3.56 and 56.8 s trend toward the Ishikari lowland

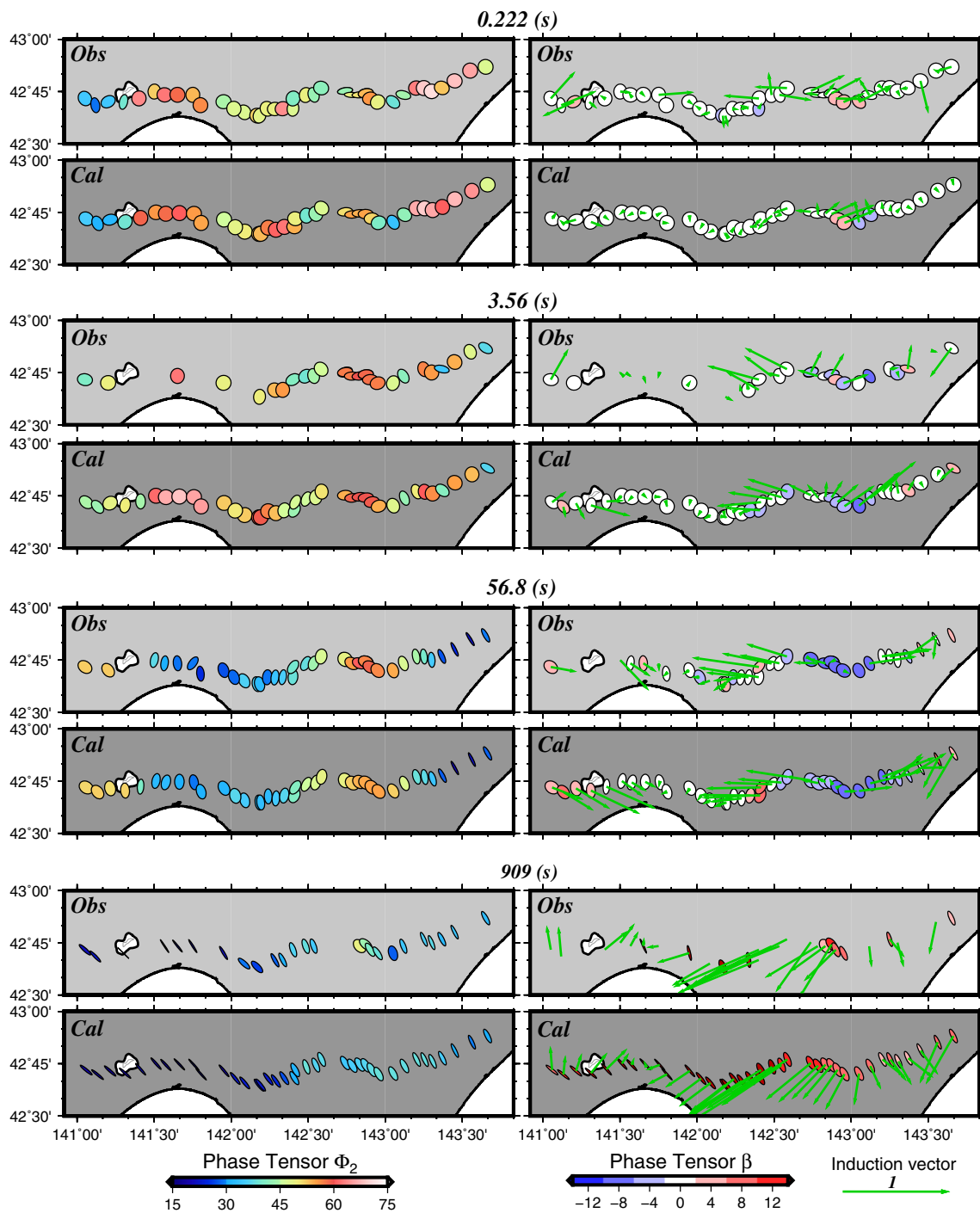


Fig. 3 Observed (OBS) and model-predicted (Cal) phase tensor ellipses and induction vectors. In the panels on the left, colored ellipses indicate Φ_2 of the phase tensor. Observed data with large errors ($\Phi_2 > 10^\circ$) are not shown. In the panels on the right, colored ellipses indicate β of the phase tensor and green arrows are Parkinson's induction vectors. Observed data with large errors ($\beta > 5^\circ$, amplitude of induction vectors > 0.05) are not shown

and the Tokachi Plain, which may indicate conductive areas there. They trend WSW with a maximum length of 0.7 at 909 s and can be attributed to current channeling

beneath the Ishikari Lowland because of the combination of conductors consisting of narrow conductive sediment beneath the lowland and seawater (Yamaya et al. 2017).

Therefore, 3-D resistivity modeling that includes the presence of seawater is necessary to correctly estimate the subsurface resistivity distribution in the study area.

3-D inversion

Although the MT stations were along a single line across the HCZ, we used 3-D rather than 2-D inversion for the following reasons. (1) The phase tensor ellipses and induction vectors (Fig. 3) indicated strong three-dimensionality of resistivity structures that 2-D modeling sometimes misinterprets. (2) 3-D inversions can provide more realistic images of resistivity structure beneath MT stations if those stations are along a single profile and the structure is strongly three-dimensional (e.g., Siripunvaraporn et al. 2005b).

We used 3-D inversion code WSINV3DMT (Siripunvaraporn and Egbert 2009; Siripunvaraporn et al. 2005a). The objective function consisting of model roughness term and data misfit term is minimized in the inversion. The former term allows to estimate broader resistivity anomaly compared to true anomaly. The inversion uses data-space formulation in the objective function and the Occam scheme to evaluate the balance of model roughness and data misfit. The settings and procedures we used are provided in Additional file 3.

The sounding curves calculated from the inverted model agreed reasonably with the measured curves (Fig. 2, Additional file 1) as did the measured phase tensor ellipses and induction vectors (Fig. 3, Additional file 2). However, high-amplitude diagonal components of MT impedance and the geomagnetic transfer function at short periods were not well resolved at several sites (Additional file 1), mainly because the horizontal mesh size of the model (> 4 km) was too large to explain small-scale horizontal variations of resistivity.

Results and discussion

The inverted resistivity model (Fig. 4a, b) shows significant resistivity variations: (1) three distinct low-resistivity anomalies (conductors) between 7 and 40 km depth on the NE Japan arc side of the HMT (C-1, C-2, and C-3), (2) two shallow conductive layers at 0–6 km depth beneath the Ishikari lowland (C-4) and Tokachi Plain (C-5), and (3) two resistive zones in the center of the HCZ (R-1 and R-2).

The anomalous conductor beneath the Shikotsu caldera (C-3) was verified by the sensitivity test, as described in Additional file 4 (see also station HDK-420 in Figs. 2, 4a, b, and Table 1). It supports the conductive region previously identified by Yamaya et al. (2017) (Additional file 5) because we used mostly different MT dataset from they used. This conductive region

possibly represents a region of magmatic fluid beneath the Shikotsu caldera as Yamaya et al. (2017) discussed. However, we do not discuss the detailed resistivity distribution in this area because Yamaya et al. (2017) modeled more-detailed resistivity distribution (see Additional file 4 for details).

Yamaya et al. (2017) detected a deep conductor beneath the Ishikari-teichi-toen fault (C1 in Yamaya et al. 2017) that our inverted resistivity model did not reproduce (Additional file 5). We attribute its absence in our model to the low sensitivity in the data due to following two effects. There is no MT site directly above the conductor. The electromagnetic field is attenuated by surface conductor C-4 and thus is slightly penetrated beneath the C-4.

The low apparent resistivities at shorter periods (Fig. 2, Additional file 1) and high Φ_2 values of the phase tensor (Fig. 3, Additional file 2) clearly suggest the presence of the two shallow subsurface conductors C-4 and C-5, which are spatially consistent with areas of low seismic velocity ($V_p < 4.5$ km/s) that were interpreted by Iwasaki et al. (2004) to represent Cretaceous or younger sedimentary rocks (Fig. 4c, d). Previous MT studies (Ichihara et al. 2008, 2016; Yamaya et al. 2017) have also recognized thick near-surface conductors associated with the sedimentary rocks.

In the following sections, we discuss our interpretations of the resistivity anomalies in the center of the HCZ (R-1, R-2, C1) and beneath the epicenter of the 2018 earthquake (C-2).

Interpretation of the conductor beneath Kamui-kotan belt (C-1)

The sensitivity tests (Additional file 4) demonstrated that the observed data require the resistivity of C-1 to be lower than 300 Ωm (Table 1) and that the C-1 anomaly possibly extended to the north of the profile (Fig. 4a). Ogawa et al. (1994) previously identified a conductor around the center of the C-1 anomaly. The distribution of the C-1 anomaly is consistent with the surface distribution of serpentinite mélangé in the Kamui-kotan belt. In addition, seismic tomographic modeling has shown an area of high attenuation of seismic energy beneath the Kamui-kotan belt (Kita et al. 2014). Such attenuation is a characteristic of rocks containing aqueous pore fluids. Thus, we interpret the C-1 anomaly to represent a zone enriched in aqueous pore fluid. Because geological studies have suggested that the root of serpentinitic material in the middle crust is in the region of C-1 (Katoh 2018; Ueda 2006), the C-1 anomaly may reflect a zone of enriched aqueous pore fluid related to the formation of serpentinite.

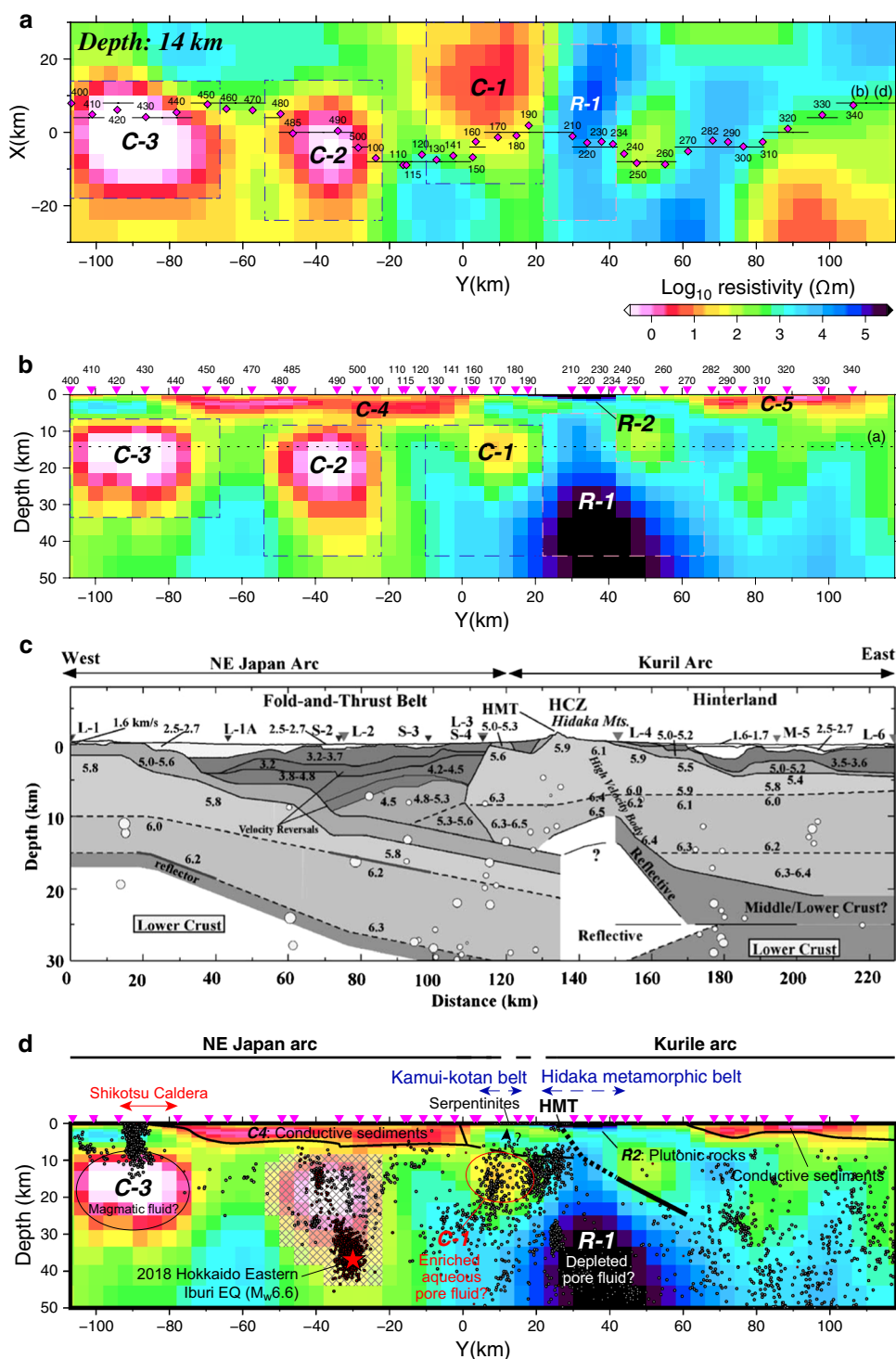


Fig. 4 Interpreted 3-D resistivity model. **a** Horizontal section of the inverted resistivity model at 14 km depth. Dashed lines show areas of sensitivity tests (where resistivity values were replaced). **b** Vertical cross-section beneath an east–west line around MT stations assembled from short east–west profiles shown as solid lines in **a**. Dotted line marks the horizontal position of **a**. **c** Interpreted seismic velocity section (from Iwasaki et al. 2004). The location of the seismic survey line corresponds closely to that of the MT survey line of this study. **d** Interpretations superimposed on the vertical cross-section of **b**. The red star denotes the hypocenter of the 2018 Hokkaido Eastern Iburi earthquake (M_w 6.6). The small circles denote hypocenters of earthquakes between 2001 and 2019. The red circles indicate hypocenters occurred after the 2018 Hokkaido Eastern Iburi earthquake. All hypocenters were determined by the Japan Meteorological Agency (2019). The C-2 is masked because of the low sensitivity

Table 1 RMS misfits obtained in sensitivity tests of the inverted electrical resistivity model

Target anomaly	Replacement value (Ωm)			
	30	100	300	1000
C-1	2.082	2.113	2.176	2.246
C-2	2.079	2.085	2.093	2.101
C-3	2.098	2.141	2.205	2.300
Target anomaly	Replacement value (Ωm)			
	1000	2000	4000	10,000
R-1	2.396	2.221	2.124	2.087

For target anomalies named with a leading “R” (or “C”), only the blocks with higher (or lower) resistivities than that shown in the “Replaced value” column were replaced. *Italic* RMS misfits indicate a model significantly different from the inverted model. The RMS misfit for the final inverted model was 2.082, and all models have 7296 degrees of freedom

Resistive bodies beneath the Hidaka metamorphic zone (R-1 and R-2)

High apparent resistivities between sites 210 and 234 (see site 230 in Fig. 2) correspond to the surface resistive zone of the Hidaka metamorphic belt (R-2), which contains granulite and plutonic rocks. The electrical resistivity of dry granulite from this area is high (2000 Ωm at 570 K; Fuji-ta et al. 2004). Moreover, dry plutonic rocks under surface conditions generally show high resistivity. Thus, the R-2 anomaly can be explained by the presence of granulite and plutonic rocks. The distribution of the eastern part of the R-2 anomaly is consistent with the distribution of plutonic rocks identified from gravity survey data (Kamiyama et al. 2005). Alternatively, the area of relatively low resistivity beneath the R-2 anomaly can be interpreted to represent metasedimentary rocks, as discussed by Kamiyama et al. (2005).

Sensitivity modeling showed that the R-1 high-resistivity anomaly (>4000 Ωm) is at depths around the middle crust (Additional file 4). Based on the surface trace of the HMT and a dipping seismic reflector previously observed in the middle crust (Iwasaki et al. 2004), the R-1 anomaly is within the footwall of the HMT (Fig. 4d). In contrast, Ichihara et al. (2016) identified a conductive zone in the footwall of the HMT in the southern part of the HCZ and interpreted it to represent dehydration fluid flow from the Pacific plate (Additional file 5). Such variations of resistivity along the footwall of the HMT possibly reflect a dependence of the supply of dehydration fluid on the depth of the plate boundary. However, resistivity distribution between the C-1 and R-1 anomalies is not constrained because of the sparse MT coverage between sites 190 and 210 (Fig. 4). More-detailed observations with a gridded array of MT sites are essential to obtain a detailed 3-D resistivity model for this anomaly.

Conductive anomaly (C-2) near the hypocenter of 2018 Hokkaido Eastern Iburi earthquake

We applied a sensitivity test (as for the C-1 anomaly) to the C-2 anomaly (see Fig. 4, Table 1, Additional file 4), which lies above the hypocenter of the 2018 Hokkaido Eastern Iburi earthquake. Yamaya et al. (2017) also showed a weak conductive anomaly in the area of our C-2 anomaly (Additional file 5). Although the sensitivity test degraded the fit of the sounding curves to the observed data (see station 490 in Fig. 2), the RMS misfit was insufficiently different from that of the final model to satisfy the *F*-test (Table 1, Additional file 4). Therefore, the observed data we used cannot resolve conductive area C-2. We suggest that attenuation of the electromagnetic field by surface conductor C-4 above the C-2 anomaly decreased the strength of the MT response of the underlying rocks.

To further clarify the resistivity distribution in the area of the C-2 anomaly, we need to increase data quality and quantity to overcome the effect of attenuation of the magnetic field by shallow conductors. The C-2 anomaly has sensitivity to the MT response around the site 490 and will be demonstrated by additional MT measurements (Additional file 4). If the modeled C-2 conductor is indeed genuine, it may represent a region rich in pore fluids that control fault rupture (e.g., Scholz 2002). It would therefore be a key to understand the anomalous faulting in the HCZ. Therefore, denser MT survey data coverage is required around the epicentral area of the 2018 Hokkaido Eastern Iburi earthquake.

Conclusions

We used 3-D inversion to reanalyze MT impedances and geomagnetic transfer functions beneath an east–west transect that crosses the HCZ and the focal zone of the 2018 Hokkaido Eastern Iburi earthquake. The resultant electrical resistivity model showed a

near-surface high-resistivity zone (R-2) beneath the Hidaka metamorphic belt that we interpreted to represent elevated mid-crustal plutonic rocks and granulite. Beneath resistive zone R-2, we identified a deep resistive zone R-1 on the footwall of the HMT, although Ichihara et al. (2016) identified conductive zones on this side of the fault in the southern part of the HCZ. The variations of resistivity we modeled possibly reflect variations of the amount of aqueous pore fluid supplied from the subducting Pacific plate. West of resistive zone R-1, we identified conductive zone C-1 beneath the high P – T metamorphic Kamui-kotan belt. Because the C-1 conductive zone is spatially related to the serpentinite mélangé of the Kamui-kotan belt, it likely represents a zone of enriched pore fluid related to the formation of the serpentinite. The resistivity model also showed a conductive anomaly (C-2) above the hypocenter of the 2018 Hokkaido Eastern Iburi earthquake; however, this anomaly was not resolved by our modeling owing to the sparse coverage and poor quality of the MT data we used. Additional dense MT surveys of high quality in the area around the epicenter of the 2018 earthquake will clarify the existence and distribution of that conductor and make an important contribution to our understanding of fault rupture processes in the deep crust in the HCZ.

Supplementary information

Supplementary information accompanies this paper at <https://doi.org/10.1186/s40623-019-1078-7>.

Additional file 1. Sounding curves. Apparent resistivity and phase of MT impedance are shown in upper and middle boxes, respectively. Tipper amplitudes are shown in lower boxes. Symbols labeled with “Obs” and “Cal” indicate observed and model-predicted MT responses, respectively.

Additional file 2. Pseudosections of observed (OBS) and model-predicted (Cal) Φ_2 (upper two panels) and β (lower two panels) of phase tensor ellipses. Observed data with large errors ($\Phi_2 > 10^\circ$, $\beta > 5^\circ$) are not shown.

Additional file 3. Settings and procedures for 3-D inversion.

Additional file 4. Verification of resistivity anomalies by sensitivity tests.

Additional file 5. Comparison of the inverted 3-D resistivity model of this study with these of Yamaya et al. (2017) and Ichihara et al. (2016).

Abbreviations

MT: magnetotelluric; HCZ: Hidaka collision zone; HMT: Hidaka main thrust.

Acknowledgements

We thank the members of the Hidaka 2000 MT observation group and Dr. Hiroyuki Kamiyama (Ueyama-shisui Co. Ltd.) for making the MT data available for this study. Continuous geomagnetic records by the Esashi geomagnetic observatory, Geospatial Information Authority of Japan, were used for remote references. Comments from Prof. H. Takahashi and Prof. Takeshi Hashimoto of Hokkaido University and two anonymous reviewers improved the manuscript. We used computer systems at the Earthquake and Volcano Information Center, Earthquake Research Institute, The University of Tokyo, for 3-D inversion and sensitivity tests. Generic Mapping Tools software (Wessel and Smith 1998) was used to draw the figures.

Authors' contributions

All authors contributed to the analyses of data and interpretation of the resistivity modeling and approved the final manuscript. All authors read and approved the final manuscript.

Funding

This research was supported in part by a grant from the Japanese Ministry of Education, Culture, Sports, Science and Technology, KAKENHI Grant no. 18K19952.

Availability of data and materials

The corresponding author can be contacted to access the digital data underpinning the 3-D resistivity model.

Ethics approval and consent to participate

Not applicable.

Consent for publication

Not applicable.

Competing interests

The authors declare that they have no competing interests.

Author details

¹ Earthquake and Volcano Research Center, Graduate School of Environmental Studies, Nagoya University, Furo-cho, Chikusa-ku, Nagoya 464-8601, Japan. ² Division of Sustainable Resources Engineering, Graduate School of Engineering, Hokkaido University, N13W8, Sapporo 060-8628, Japan. ³ Volcanic Fluid Research Center, School of Science, Tokyo Institute of Technology, Tokyo, Japan. ⁴ Nuclear Regulation Department, Secretariat of Nuclear Regulation Authority, 1-9-9, Roppongi, Minato-ku, Tokyo 106-8450, Japan. ⁵ Renewable Energy Research Center, Fukushima Renewable Energy Institute, AIST, 2-2-9 Machiikedai, Koriyama, Fukushima 963-0298, Japan.

Received: 5 March 2019 Accepted: 26 August 2019

Published online: 18 September 2019

References

- Amante C, Eakins BW (2009) ETOPO1 1 Arc-minute global relief model: procedures, data sources and analysis. NOAA Technical Memorandum NESDIS NGDC-24. National Geophysical Data Center, NOAA. <https://doi.org/10.7289/v5c8276m>
- Caldwell TG, Bibby HM, Brown C (2004) The magnetotelluric phase tensor. *Geophys J Int* 158:457–469
- Fuji-ta K, Katsura T, Tainosho Y (2004) Electrical conductivity measurement of granulite under mid- to lower crustal pressure–temperature conditions. *Geophys J Int* 157:79–86
- Gamble TD, Clarke J, Goubau WM (1979) Magnetotellurics with a remote magnetic reference. *Geophysics* 44:53–68
- Heise W, Pous J (2003) Anomalous phases exceeding 90° in magnetotellurics: anisotropic model studies and a field example. *Geophys J Int* 155:308–318
- Ichihara H, Mogi T (2009) A realistic 3-D resistivity model explaining anomalous large magnetotelluric phases: the L-shaped conductor model. *Geophys J Int* 179:14–17. <https://doi.org/10.1111/j.1365-246X.2009.04310.x>
- Ichihara H, Honda R, Mogi T, Hase H, Kamiyama H, Yamaya Y, Ogawa Y (2008) Resistivity structure around the focal area of the 2004 Rumoi-Nanbu earthquake (M 6.1), northern Hokkaido, Japan. *Earth Planets Space* 60:883–888. <https://doi.org/10.1186/Bf03352841>
- Ichihara H, Mogi T, Yamaya Y (2013) Three-dimensional resistivity modelling of a seismogenic area in an oblique subduction zone in the western Kurile arc: constraints from anomalous magnetotelluric phases. *Tectonophysics* 603:114–122. <https://doi.org/10.1016/j.tecto.2013.05.020>
- Ichihara H, Mogi T, Tanimoto K, Yamaya Y, Hashimoto T, Uyeshima M, Ogawa Y (2016) Crustal structure and fluid distribution beneath the southern part of the Hidaka collision zone revealed by 3-D electrical resistivity modeling. *Geochem Geophys Geosyst* 17:1480–1491. <https://doi.org/10.1002/2015gc006222>

- Iwasaki T, Adachi K, Moriya T, Miyamachi H, Matsushima T, Miyashita K, Takeda T, Taira T, Yamada T, Ohtake K (2004) Upper and middle crustal deformation of an arc–arc collision across Hokkaido, Japan, inferred from seismic refraction/wide-angle reflection experiments. *Tectonophysics* 388:59–73
- Japan Meteorological Agency (2019) The seismological Bulletin of Japan. http://www.data.jma.go.jp/svd/eqev/data/bulletin/index_e.html. Accessed 8 June 2019
- Kamiyama H, Yamamoto A, Hasegawa T, Kajiwara T, Mogi T (2005) Gravity and density variations of the tilted Tottabetsu plutonic complex, Hokkaido, northern Japan: implications for subsurface intrusive structure and pluton development. *Earth Planets Space* 57:E21–E24. <https://doi.org/10.1186/BF03351894>
- Kato N, Sato H, Orito M, Hirakawa K, Ikeda Y, Ito T (2004) Has the plate boundary shifted from central Hokkaido to the eastern part of the Sea of Japan? *Tectonophysics* 388:75–84
- Katoh T (2018) A geological east-west cross section through the Iwanai-dake peridotite mass in Hidaka town based on the tectogenesis of ultramafic masses, Hokkaido. *Bull Hidaka Mt Mus Hidaka Mt Res* 1:21–30
- Kimura G (1986) Oblique subduction and collision—Fore-arc tectonics of the Kuril Arc. *Geology* 14:404–407. [https://doi.org/10.1130/0091-7613\(1986\)14%3c404:Osacft%3e2.0.Co;2](https://doi.org/10.1130/0091-7613(1986)14%3c404:Osacft%3e2.0.Co;2)
- Kita S, Hasegawa A, Nakajima J, Okada T, Matsuzawa T, Katsumata K (2012) High-resolution seismic velocity structure beneath the. *J Geophys Res-Solid Earth*. <https://doi.org/10.1029/2012jb009356>
- Kita S, Nakajima J, Hasegawa A, Okada T, Katsumata K, Asano Y, Kimura T (2014) Detailed seismic attenuation structure beneath Hokkaido, northeastern Japan: Arc-arc collision process, arc magmatism, and seismotectonics. *J Geophys Res-Solid Earth* 119:6486–6511. <https://doi.org/10.1002/2014jb011099>
- Mogi T, Hidaka 2000 MT Group (2002) Broadband MT surveys in Hidaka area. *Monthly Chikyū* 24:485–487 (in Japanese)
- Ogawa Y, Nishida Y, Makino M (1994) A collision boundary imaged by magnetotellurics, Hidaka Mountains, Central Hokkaido, Japan. *J Geophys Res-Solid Earth* 99:22373–22388
- Parkinson WD (1962) The influence of continents and oceans on geomagnetic variations. *Geophys J R Astron Soc* 6:441–449
- Pek J, Verner T (1997) Finite-difference modelling of magnetotelluric fields in two-dimensional anisotropic media. *Geophys J Int* 128:505–521
- Scholz CH (2002) *The mechanics of earthquakes and faulting*, 2nd edn. Cambridge University Press, Cambridge
- Sibson RH (1990) Rupture nucleation on unfavorably oriented faults. *Bull Seismol Soc Am* 80:1580–1604
- Siripunvaraporn W, Egbert G (2009) WSINV3DMT: vertical magnetic field transfer function inversion and parallel implementation. *Phys Earth Planet Interiors* 173:317–329. <https://doi.org/10.1016/J.Pepi.2009.01.013>
- Siripunvaraporn W, Egbert G, Lenbury Y, Uyeshima M (2005a) Three-dimensional magnetotelluric inversion: data-space method. *Phys Earth Planet Interiors* 150:3–14
- Siripunvaraporn W, Egbert G, Uyeshima M (2005b) Interpretation of two-dimensional magnetotelluric profile data with three-dimensional inversion: synthetic examples. *Geophys J Int* 160:804–814
- Ueda H (2006) Geologic structure of Cretaceous accretionary complexes in the frontal Hidaka collision zone, Hokkaido, Japan. *J Geol Soc Jpn* 112:699–717
- Wessel P, Smith WHF (1998) New, improved version of Generic Mapping Tools released. *EOS Trans Am Geophys Union* 79(47):579
- Yamaya Y, Mogi T, Honda R, Hase H, Hashimoto T, Uyeshima M (2017) Three-dimensional resistivity structure in Ishikari Lowland, Hokkaido, northeastern Japan—implications to strain concentration mechanism. *Geochem Geophys Geosyst* 18:735–754. <https://doi.org/10.1002/2016gc006771>

Publisher's Note

Springer Nature remains neutral with regard to jurisdictional claims in published maps and institutional affiliations.

Submit your manuscript to a SpringerOpen[®] journal and benefit from:

- Convenient online submission
- Rigorous peer review
- Open access: articles freely available online
- High visibility within the field
- Retaining the copyright to your article

Submit your next manuscript at ► springeropen.com
